The Plant Journal (2004) **38**, 526–538 doi: 10.1111/j.1365-313X.2004.02065.x

DISTORTED2 encodes an ARPC2 subunit of the putative *Arabidopsis* ARP2/3 complex

Salah El-Din El-Assal[1], Jie Le[1], Dipanwita Basu[1] Eileen L. Mallery[1] and Daniel B. Szymanski[1,2,*]
[1]*Agronomy Department, Purdue University, Lilly Hall, 915 West State Street, West Lafayette, IN 47907-2054, USA, and*
[2]*Purdue Motility Group, Purdue University, Lilly Hall, 915 West State Street, West Lafayette, IN 47907-2054, USA*

Received 16 September 2003; revised 16 January 2004; accepted 10 February 2004.
*For correspondence (fax +1 765 496 7255; e-mail dszyman@purdue.edu).

Summary

***Arabidopsis* trichomes are unicellular, branched structures that have highly constrained requirements for the cytoskeleton. The 'distorted group' genes function downstream from microtubule-based branch initiation, and are required during the actin-dependent phase of polarized stalk and branch expansion. Of the eight known 'distorted group' genes, a subset encode homologs of ARP2/3 complex subunits. In eukaryotic cells, the seven-protein ARP2/3 complex nucleates actin filament networks that push on the plasma membrane and organelles. In plants cells, the existence and function of an ARP2/3 complex is unclear. In this paper, we report that *DISTORTED2* (*DIS2*) encodes a paralogue of the ARP2/3 complex subunit ARPC2. DIS2 has ARPC2 activity, based on its ability to rescue the growth defects of *arpc2* (*arc35Δ*) null yeast cells. Like known ARPC2s, DIS2 physically interacts with ARPC4. Mutations in *DIS2* cause a distorted trichome phenotype, defects in cell–cell adhesion, and a modest reduction in shoot FW. The actin cytoskeleton in *dis2* trichomes is extensive, but developing branches fail to generate and maintain highly organized cytoplasmic actin bundles.**

Keywords: ARP2/3, actin, cytoskeleton, trichome, distorted, ARPC2, cell adhesion.

Introduction

In growing plant cells, the actin cytoskeleton is required to maintain transvacuolar cytoplasm, to position the endoplasmic reticulum, and to facilitate polarized intracellular trafficking (reviewed by Staiger, 2000). The use of *Arabidopsis* molecular genetics and trichome morphology mutants is yielding new information about how the cytoskeleton is organized and its function (reviewed by Wasteneys and Galway, 2003). *Arabidopsis* leaf trichomes are approximately 400-μm-long, unicellular, branched structures that have distinct requirements for the microtubule and actin cytoskeletons. Based on genetic (Burk *et al.*, 2001; Kirik *et al.*, 2002; Oppenheimer *et al.*, 1997) and pharmacological (Mathur *et al.*, 1999; Szymanski *et al.*, 1999) data, microtubules function both during branch initiation and at later stages of development (Szymanski, 2001). The concentration of circumferential microtubules in the apical regions of newly formed stalks and branches is consistent with microtubule-based control of the earliest phases of branch morphogenesis (Folkers *et al.*, 2002). Although the actin cytoskeleton is extensive throughout trichome development, inhibitor experiments first detect a requirement for actin cytoskeleton during stage 4 (defined in Szymanski *et al.*, 1998) following branch initiation (Szymanski *et al.*, 1999). The branches of stage 4 cells contain both a fine cortical actin meshwork and cytoplasmic bundles that are loosely aligned with the long axis of the branch (Le *et al.*, 2003; Szymanski *et al.*, 1999). The precise function of the actin cytoskeleton during trichome growth is not known, but in other cell types, the presence of fine cortical actin filaments is correlated with regions of active cell expansion (Blancaflor, 2000; Foissner *et al.*, 1996; Miller *et al.*, 1999), and actin bundles mediate organelle positioning and transport (Boevink *et al.*, 1998; Nebenfuhr *et al.*, 1999). The distorted mutants have clear actin-based phenotypes and trichome-shaped defects that are indistinguishable from wild-type cells that are treated with actin-disrupting drugs (Schwab *et al.*, 2003; Szymanski *et al.*, 1999). Collectively, the 'distorted group' of trichome mutants is a useful set of mutants to study actin-dependent growth mechanisms in plants.

Recently, three 'distorted group' genes (*DISTORTED1* (*DIS1*), *WURM* (*WRM*), and *CROOKED* (*CRK*)) have been

shown to encode homologs of ARP2/3 complex subunits (Le *et al.*, 2003; Li *et al.*, 2003; Mathur *et al.*, 2003b). The ARP2/3 complex is an evolutionarily conserved, seven-protein complex that was originally purified from *Acanthamoeba* (Machesky *et al.*, 1994). In an activated state, the ARP2/3 complex binds to the sides of existing actin filaments ('mother' filaments) and efficiently nucleates 'daughter' filaments (Amann and Pollard, 2001; Blanchoin *et al.*, 2000). ARP2/3-containing dendritic networks of actin filaments facilitate both plasma membrane protrusion and filopodia formation at the leading edge of migrating cells and drive the motility of a variety of organelles and intracellular pathogens (reviewed by Schafer, 2002; Welch and Mullins, 2002). Although each of the seven ARP2/3 subunit-like genes is expressed in *Arabidopsis* (Li *et al.*, 2003), there is no biochemical data to support the existence of a seven-protein complex in plants.

Genetic data indicate the ARP2/3 complex is essential in yeast (Lees-Miller *et al.*, 1992; Winter *et al.*, 1999), *Drosophila* (Hudson and Cooley, 2002), and *Caenorhabditis elegans* (Sawa *et al.*, 2003). However, not all ARP2/3 subunit genes make equal functional contributions. For example, in *Saccharomyces cerevisiae*, deletion of the *arc40* (*arpc1*) and *arc35* (*arpc2*) cause lethality and severe reductions in viability, respectively. In contrast, 88% of the spores that lack an *Arc18* (*ARPC3*) gene are viable and grow at nearly wild-type rates (Winter *et al.*, 1999). Reconstitution of recombinant ARP2/3 complexes *in vitro* confirmed the importance of the ARPC2–ARPC4 dimer as the core, actin-binding element onto which the other subunits assemble (Gournier *et al.*, 2001). Given the severe growth defects of ARP2/3 subunit mutants in other species, the mild phenotypes of the 'distorted group' mutants is somewhat surprising. Although predicted null alleles of *wrm* (*ARP2*) and *dis1* (*ARP3*) affect the shape of a variety of cell types and reduce total shoot growth rates, the overall architecture of mature plants is not affected (Le *et al.*, 2003). Trichomes with predicted null mutations in *ARP2* and *ARP3* genes also contain an extensive actin cytoskeleton, the organization of which has been described as excessively bundled by Li *et al.* (2003) and Mathur *et al.* (2003a,b) or improperly aligned by Le *et al.* (2003). The precise relationship between actin filament organization and ARP2/3 subunit function in trichomes remains to be resolved.

This paper extends our knowledge concerning the functional requirements for an ARPC2-like gene during multicellular development. Stringent molecular genetic tests demonstrate that *DIS2* encodes a paralog of the ARPC2 subunit. Overexpression of *DIS2* rescues the growth defects of *arc35* (*aprc2*) null *S. cerevisiae* strain. A conserved physical interaction between known ARPC2 and ARPC4 subunits also occurs between DIS2 and ATARPC4. In addition to stage-specific trichome swelling, *dis2* plants have defective cell–cell adhesion and a modest decrease in FW. The *dis2* trichomes, like those of other 'distorted group' mutants, have an extensive actin cytoskeleton. However, *dis2* trichomes display clear defects in the generation and maintenance of aligned actin bundles in the core cytoplasm of the branches.

Results

Molecular characterization of DIS2

All 'distorted group' mutants identified to date have trichomes that are similar to the wild type (Figure 1a) until after branch formation occurs (stage 4). In addition to the known *dis2-1* allele (Feenstra, 1978), we isolated two new recessive alleles in the Columbia (Col-0) background. The new *dis2* alleles displayed stage-specific swelling and reduced branch length that was indistinguishable from *dis2-1* (Figure 1b–f). The terminal phenotype of the *dis2-1* trichomes was variable, and included comparable numbers of cells with one highly polarized branch (Figure 1c), an

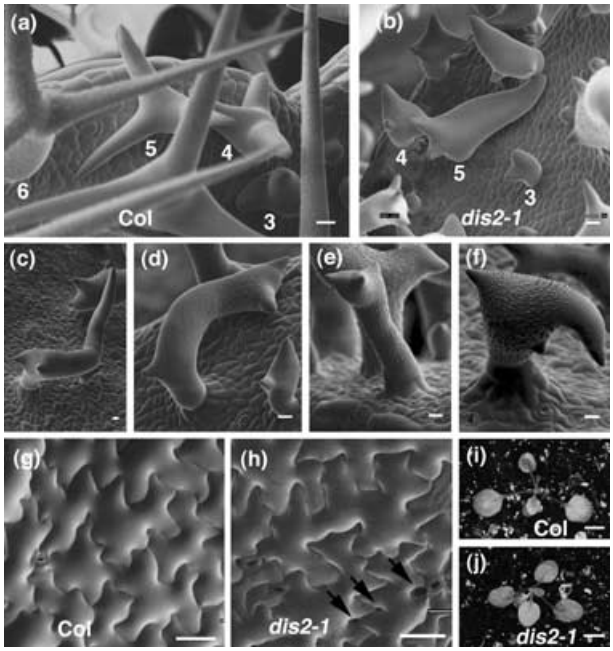

Figure 1. Comparison of the trichome, pavement cells, and shoot phenotypes of the wild type and *dis2-1*.
(a) Upper surface of developing wild-type leaves.
(b) Upper surface of developing *dis2-1* leaves.
(c–f) The variable shapes of mature *dis2-1* trichomes.
(g) Upper surface of 12 DAG wild-type cotyledon pavement cells.
(h) Upper surface of 12 DAG *dis2-1* cotyledon pavement cells.
(i) Wild-type seedling (13 DAG).
(j) *dis2-1* seedling (13 DAG).
Numbers in panels (a) and (b) indicate the developmental stage of trichomes. Arrows indicate the gaps between adjacent pavement cells in panel (h). Bars: (a–f) 10 μm; (g,h) 50 μm; (i,j) 4 mm.

abnormally expanded interbranch zone, which is defined as the stalk-like region of the cell that spans the branch attachment points (Figure 1d), and cells with three abortive branches positioned at the apical region of the cell (Figure 1e). Some trichomes were abnormally swollen at multiple locations (Figure 1f).

Each of the *dis2* mutations caused cell–cell adhesion defects. Hypocotyl and pavement cell adhesion defects also occur in *dis1*, *wrm*, and *crk* (Le *et al.*, 2003; Mathur *et al.*, 2003a,b). Wild-type cotyledon epidermal pavement cells have an intricate lobed morphology that interdigitate smoothly with neighboring cells (Figure 1g). In the wild type, clear gaps between adjacent cells were extremely rare under any growth condition. The lobed morphology of *dis2* pavement cells was noticeably different from that of the wild type; however, gaps between adjacent cells were observed consistently (Figure 1h). The cotyledon epidermal adhesion defects of *dis2* plants were more severe when the plants were grown *in vitro* (data not shown), probably because of increased viability or tolerance of cell adhesion defects when the plants were grown at 100% humidity. Hypocotyl length of light-grown *dis2* mutants did not differ significantly from that of the wild type (data not shown). However, the mean hypocotyl length of *dis2-1* (6.1 ± 0.8 mm; $n = 8$) etiolated seedlings was less than half of the mean length of the wild type (15 ± 0.8 mm; $n = 8$). Hypocotyl epidermal cells in *dis2-1* etiolated seedlings had defective cell–cell adhesion relative to the wild type (Supplementary Material; Figure S1). The relationship between the actin cytoskeleton and end-to-end cell adhesion has been examined in detail by Mathur *et al.* (2003b).

Although the whole plant architecture of each of the *dis2* alleles was indistinguishable from that of the wild type (Figure 1i,j), FW measurements taken from segregating populations consistently revealed a trend of reduced FW in *dis2-1* and *dis2-2* plants. In one experiment, *dis2-1* (112 ± 3 mg, $n = 5$) plants weighed approximately 15% less than the wild type (131 mg $\pm$ 20, $n = 6$) segregants from the same F_2 population. As a standard for comparison, *dis1* plants weigh approximately 35% less than wild-type controls (Le *et al.*, 2003). Root hair and pollen tube growth have strict requirements for the actin cytoskeleton (Baluska *et al.*, 2000; Gibbon *et al.*, 1999). Neither root hair morphogenesis nor the fertility of *dis2* plants was dramatically affected, suggesting that neither of these cell types had strict requirements for *DIS2* function.

In order to clone the *DIS2* gene, we generated a mapping population by crossing *dis2-1* (Landsberg *erecta* (L*er*)) to Col-0. Consistent with its published position on the classical genetic map, *dis2-1* mapped to within approximately 1 cM of marker S0392 on chromosome 1 (Figure 2a). Genotyping of the recombinant chromosomes with the marker UFO positioned *DIS2* south of S0392. We sequenced the *ATARPC2A* gene that was located near the predicted location of *DIS2*. *dis2-1* had a G to A transition at the conserved splice donor sequence following exon 5 (Figure 2b). The *dis2-1* mutation caused the accumulation of two mis-spliced transcripts (Figure 2c, lane 3). The unspliced *dis2-1* transcript (*dis2-1U*) retained intron 4, but efficiently spliced the other introns. *dis2-1U* encoded 188 amino acids of *DIS2*, and then three nonsense amino acids, before a stop codon was encountered. The spliced *dis2-1* transcript (*dis2-1S*) was generated by aberrant splicing in which the splice donor of exon 4 and the splice acceptor of exon 6 were used, resulting in the removal of exon 5 and the predicted deletion of amino acids 166–191. The *dis2-2* and *dis2-3* alleles both contained G to A transitions at base pairs +1571 and +1572, respectively. (The numbering is relative

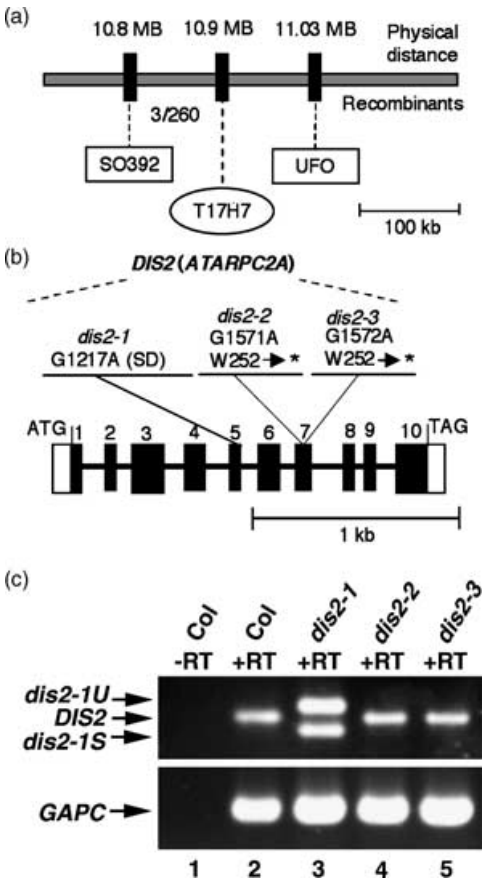

Figure 2. Mapping and molecular characterization of *DIS2* mutant alleles.
(a) Mapping of the *DIS2* gene. Boxes indicate the position of molecular markers, and the oval represents the *DIS2*-containing BAC (T17H7). Recombination frequency is given.
(b) Physical structure of the *DIS2* gene. The position of exons and introns are indicated by black rectangles and lines, respectively. The 5′ and 3′ UTRs are indicated by white rectangles. The location and nature of the *dis2-1*, *dis2-2*, and *dis2-3* mutations are labeled. SD, splice donor.
(c) RT-PCR of *DIS2* gene in wild-type and different mutant backgrounds using primers C2F and C2R. Specific primers for *GAPC* gene were used as a control. Lane 1, no reverse transcriptase (−RT) control; lane 2, plus (+) RT control; lane 3, *dis2-1* (+RT); lane 4, *dis2-2* (+RT); lane 5, *dis2-3* (+RT).

to the experimentally supported transcription start site that can be viewed using SEQVIEWER for AT1G30825 at http://www.arabidopsis.org). Both alleles changed the same UGG codon to two different stop codons (W252*). The failure of *dis2-2* and *dis2-3* to complement *dis2-1* in crosses, the allele sequencing results, and the measured defects in *dis2-1* mRNA processing provide very strong evidence that *DIS2* corresponded to the *ATARPC2A* gene. As additional proof for gene identity, we rescued the *dis2* phenotype by overexpressing the *DIS2* cDNA using the strong 35S viral promoter. Fifteen of 15 transformed *dis2* plants that carried the overexpression transgene displayed a wild-type trichome morphology (data not shown). For the remainder of this paper, *ATARPC2A* will be referred to as *DIS2*.

A full-length *DIS2* cDNA clone (GenBank Accession: AK118475) was publicly available (Seki *et al.*, 2002). We confirmed the sequence of the *DIS2* full-length clone and used two expressed sequence tag (EST) sequences containing the *DIS2* 5′ untranslated region (UTR) and three ESTs containing the 3′ UTR to generate the gene model shown in Figure 2. The *DIS2* cDNA contained a single open-reading frame that encoded a predicted 36-kDa polypeptide of 318 amino acids (Figure 3). The putative ARPC2 orthologs from plant, insect, nematode, and vertebrate species shared approximately 30% identity with *S. cerevisiae* ARPC2. The homology with *S. cerevisiae* ARPC2 was higher in the C-terminal 120 amino acids, with each of the ARPC2-encoding genes sharing between 37–40% identity in this region.

DIS2 is not the only *ARPC2*-like gene in *Arabidopsis* (Le *et al.*, 2003). BLASTP database searches using the deduced ARPC2 amino acid sequences from a variety of species consistently identified a second *ARPC2*-like gene in *Arabidopsis* (*ATARPC2B*) and rice (*OSARPC2B*). The ARPC2B proteins had a slightly lower level of amino acid identity with other ARPC2s because of a C-terminal extension of approximately 60 amino acids (relative to vertebrate ARPC2) (Figure 3). The C-terminal extension of OSARPC2B and ATARPC2B was very basic, with more than 30% of the residues consisting of either lysine (K) or arginine (R). A more conventional rice ARPC2-like protein (*OSARPC2A*) that lacked the basic C-terminal extension was also predicted from the rice genome sequence (Figure 3). The evolutionary relationships between rice and *Arabidopsis ARPC2*-like genes were examined more closely by aligning the plant sequences with ARPC2s from diverse species. The manually edited CLUSTALW alignment shown in Figure 3 was used as an input to generate an unrooted phylogenetic tree using parsimony (Supplementary Material, Figure S2).

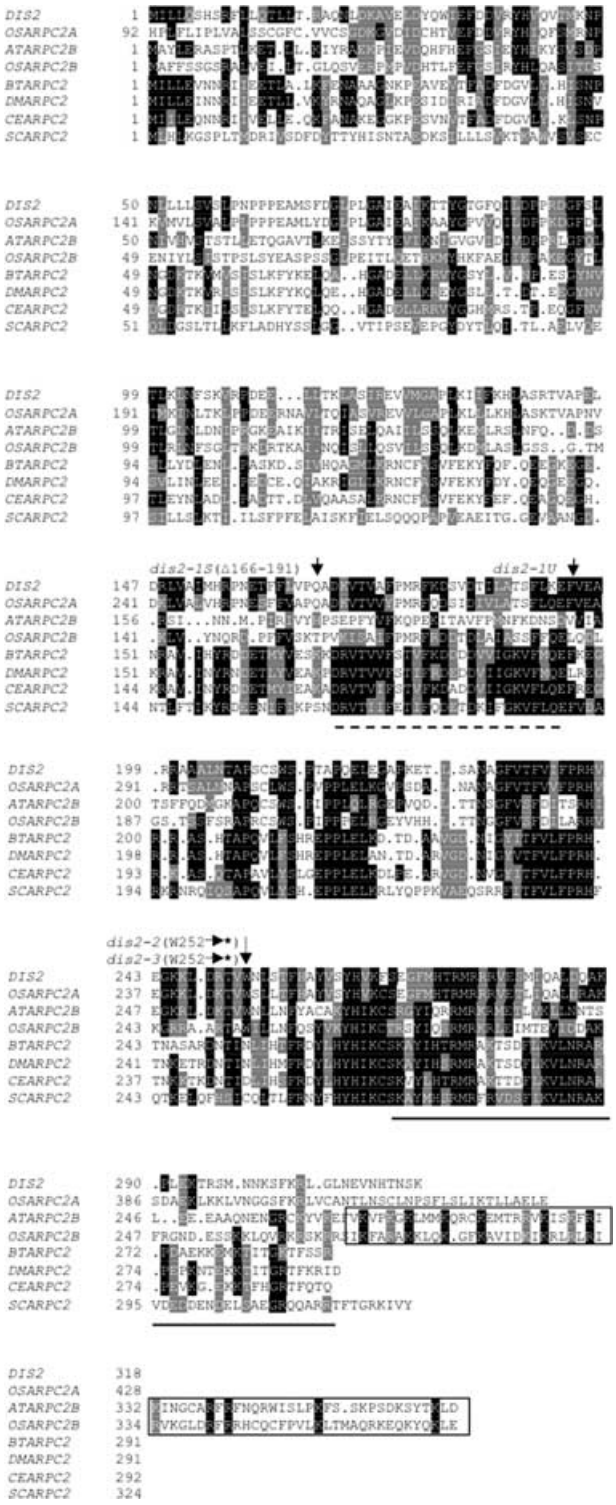

Figure 3. Amino acid sequence comparisons among *Arabidopsis* DIS2 and ARPC2s from other species.

The positions of the last correct amino acid before mis-splicing of *dis2-1S* (spliced mRNA), *dis2-1U* (unspliced mRNA) and the premature stop codon of *dis2-2* and *dis2-3* are labeled. The deleted amino acids in *dis2-1S* are labeled with a dashed line. The C-terminal alpha-helix of 43 residues of BTARPC2 that associates with ARPC4 (p20) is underlined. The conserved C-terminal domains of *Arabidopsis* and rice ARPC2Bs are boxed with conserved basic amino acids shaded. Amino acid residues in black indicate identity, and those in gray indicate conserved substitutions. DIS2 (BT005308), ATARPC2B (NM_179877), *O. sativa* OSARPC2A (AP003709), OSARPC2B (CAE03390), *B. taurus* BTARPC2 (1K8K_D), *D. melanogaster* DMARPC2 (NP_610033), *C. elegans* CEARPC2 (NP_741088) and *S. cerevisiae* SCARPC2 (NP_014433).

Bootstrapping analysis strongly supported the phylogenetic model in which the *Arabidopsis* and rice *ARPC2A* and *ARPC2B* genes form separate clades.

We next used yeast mutant rescue experiments and the yeast two-hybrid assay to test for functional similarities between *DIS2* and known *ARPC2*s. *S. cerevisiae* cells that are null for *ARPC2* (*arc35Δ*) are slow growing, and the cells fail to separate normally following cytokinesis (Winter *et al.*, 1999). Overexpression of *DIS2* in *arc35Δ* cells using a galactose-inducible promoter rescued both phenotypes (Figure 4a). The rescue required the wild-type *DIS2* coding sequences because neither the overexpression of *dis2-1S* nor an empty vector control had significant activity (Figure 4a). The known physical interaction between

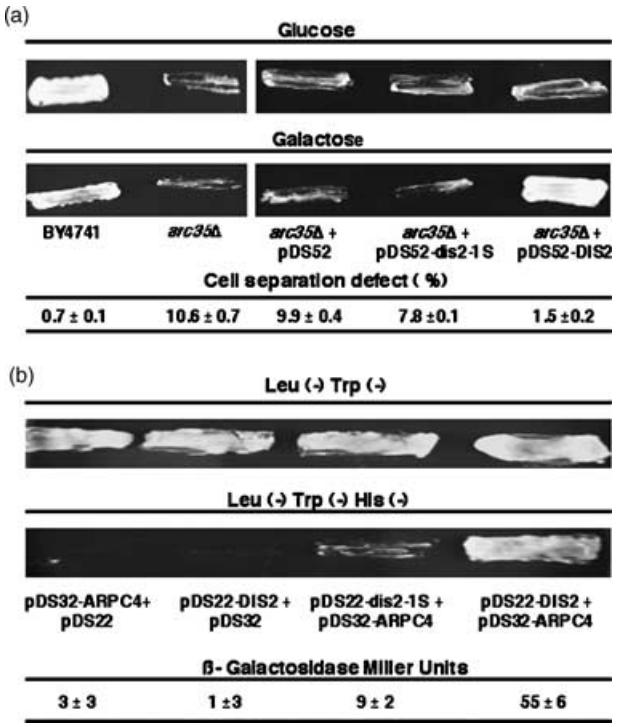

Figure 4. DIS2 can function as an ARPC2 in yeast, and retains a conserved physical interaction with ATARPC4.
(a) Rescue of growth defects of *S. cerevisiae arc35Δ* with *Arabidopsis DIS2*. Upper left, *S. cerevisiae* patches of haploid wild-type strain BY4741 and untransformed *arc35Δ*; upper right, patches of *arc35Δ* transformed with: an empty vector control (pDS52), a plasmid expressing the *dis2-1S* allele (pDS52-dis2-1S), and a plasmid expressing the wild-type *DIS2* (pDS52-DIS2). All strains in the upper panel were grown on glucose-containing plates. Lower, same strains as above, but struck on galactose inducer-containing plates. The numbers listed below each strain are the percentage of unseparated cells in saturated cultures ($n > 80$ in all cases).
(b) Interaction of DIS2 and ATARPC4 in a yeast two-hybrid assay. Upper, patches of *S. cerevisiae* Y190 strain co-transformed with: (i) an ATARPC4-bait (pDS32-ARPC4) and an empty vector control (pDS22); (ii) DIS2-prey (pDS22-DIS2) and an empty vector control (pDS32); (iii) the *dis2-1S*-prey (pDS22-dis2-1S) and ARPC4-bait; and (iv) DIS2-prey and ARPC4-bait. All strains in the upper panel were plated on Leu$^-$ Trp$^-$ plates. Lower, same strains as (a), but struck on Leu$^-$ Trp$^-$ His$^-$ plates. Numbers below each strain are the quantitative analysis of the β-galactosidase activity of each strain.

ARPC2 and ARPC4 (Gournier *et al.*, 2001; Zhao *et al.*, 2001) also occurred between DIS2 and ATARPC4 in a yeast two-hybrid assay (Figure 4b). Strains that harbored both the ATARPC4 as bait and DIS2 as prey grew on His$^-$ plates and activated the β-Gal reporter gene (Figure 4b). Experiments that paired either pDS32-ARPC4 or pDS22-DIS2 with empty vector controls demonstrated that both *DIS2* and *ATARPC4* coding sequences are needed to activate the reporter genes. The *dis2-1* transcripts encode a truncated protein (dis2-1U) and one that deletes 26 amino acids from the middle of the sequence (dis2-1S). In Western blots of yeast extracts, the dis2-1U fusion protein was unstable, but the accumulation of dis2-1S and DIS2 fusion proteins was not significantly different (data not shown). In the two-hybrid assay, dis2-1S interacted weakly with ATARPC4, and activated the β-Gal approximately sixfold less than the wild-type protein.

We wanted to determine whether *DIS2*, *ATARPC2B*, and *ATARPC4* had similar expression patterns. The ARP2/3 subunit-like genes are expressed in all major organs with the highest level of expression in inflorescences (Li *et al.*, 2003). We also analyzed *DIS1* (*ARP3*) and *WRM* (*ARP2*) expression to compare our results with published data. The threshold for detection of each transcript using reverse transcriptase-PCR (RT-PCR) for each primer pair was 18 or 19 PCR cycles, and the data shown in Figure 5 was generated using 20-cycle reactions. Amplification of the glyceraldehyde 3-phosphate dehydrogenase (*GAPC*) was used as a control for the amount of input cDNA for each PCR reaction. Controls lacking RT were conducted on all RNA samples to demonstrate the absence of contaminating DNA. The result of a seedling control experiment lacking RT is shown in Figure 5, lane 1. *WRM*, *DIS1*, *DIS2*, and *ATARPCB* were expressed in roots hypocotyls, cotyledons, leaves, stems, inflorescences, and flowers. The relative expression levels of each ARP2/3 subunit-like gene in cotyledons were the same at 5 and 15 days after germination (DAG), and in leaves at different developmental stages (data not shown). Consistent with the results of Li *et al.* (2003), the relative expression levels for each of the ARP2/3 complex subunit-like genes were highest in inflorescences. The level of *DIS2* and *ATARPC2B* expression was lower than the other subunit-like genes (Figure 5c,d). *ATARPC4* was expressed at high levels in most of the organs, but like *CRK* (ARPC5) and *ATARPC3* (Li *et al.*, 2003), it was expressed at higher levels in stems relative to leaves (Figure 5e). Other ARP2/3 subunit genes are expressed at the lowest level in stems (Figure 5a–c).

Actin localization in wild-type and dis2 *trichomes at key developmental stages*

In order to test for an effect of *dis2* on the actin cytoskeleton, we focused our efforts on localizing the actin cytoskeleton

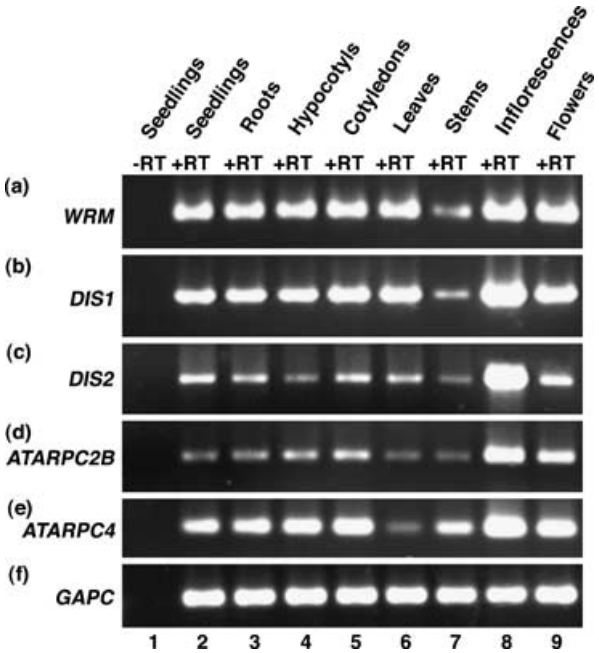

Figure 5. RT-PCR analysis of ARP2/3 complex subunit-like gene expression in different organs.
(a) *WRM* (*ATARP2*).
(b) *DIS1* (*ATARP3*).
(c) *DIS2* (*ATARPC2A*).
(d) *ATRPC2B*.
(e) *ATARPC4*.
(f) *GAPC* control.
Lane 1, no reverse transcriptase (−RT) in five DAG seedlings; lane 2, plus (+) RT in five DAG seedlings; lane 3, five DAG roots (+RT); lane 4, five DAG hypocotyls (+RT); lane 5, five DAG cotyledons (+RT); lane 6, 15 DAG leaves (+RT); lane 7, stem (+RT); lane 8, inflorescences (+RT); lane 9, flowers (+RT).

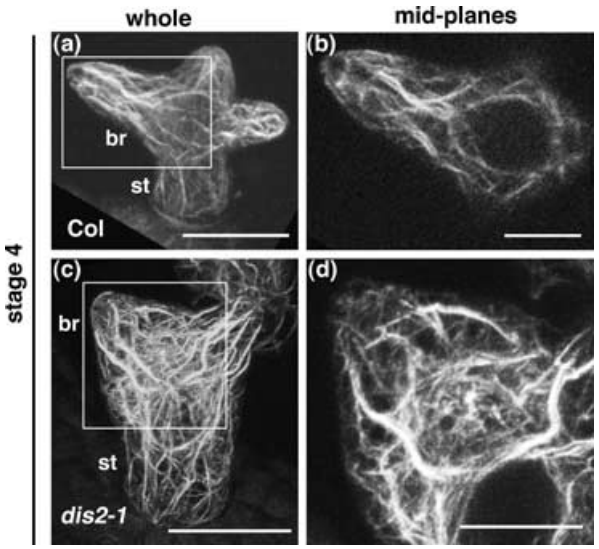

Figure 6. Localization of actin filaments in whole-mounted wild-type and *dis2-1* stage 4 trichomes.
(a) Wild type, maximum projection of all planes.
(b) Wild type, high magnification of the boxed region of (a). The image is a maximum projection of the core cytoplasmic space.
(c) *dis2-1*, maximum projection of all planes.
(d) *dis2-1*, high magnification of the boxed region in (c). The image is a maximum projection of the core cytoplasm of the branch and stalk.
Bars: (a,c) 20 μm; (b,d) 10 μm. br, Branch; st, stalk.

at the onset of the mutant phenotype immediately following branch initiation (stage 4). The images in Figures 6–8 reflect consistently observed actin localization patterns obtained using Alexa-488 phalloidin, which yields results similar to those of freeze shattering and antibody labeling (Le *et al.*, 2003). There are no published images of actin filaments in stage 4 trichomes using GFP:talin, and in our hands, this probe does not label actin in stage 4 or younger cells (D. Szymanski and J. Le, unpublished results). Phalloidin-labeled wild-type stage 4 cells contained both a cortical meshwork of actin filaments and a population of longitudinally oriented bundles in the central region of the branch cytoplasm (Figure 6a). Many of the core cytoplasmic actin bundles converge at specific locations in the cell and terminate cleanly (Figure 6b). Similarly staged *dis2-1* cells contained a cortical actin meshwork and a population of bundles deeper in the cytoplasm (Figure 6c,d). Although *dis2-1* branches frequently contained a few longitudinally oriented bundles in the core cytoplasm that extended toward the branch tip, the vast majority were oriented randomly and terminated at various locations in the branch and stalk (Figure 6d). Similar disorganization of cytoplasmic bundles was observed in stage 4 *dis2-2* trichomes (data not shown), and in stage 4 *dis1* and *grl* trichomes (Le *et al.*, 2003; Szymanski *et al.*, 1999).

We next tested *dis2-1* for a difference in the relative amount of actin filaments in the core cytoplasm in stage 3/4 and stage 4/5 branches. For these measurements, it is important to exclude highly expanded, late stage 5 and stage 6 mutant cells with abortive branches. Therefore, in addition to branch length criteria, we limited our analysis of *dis2-1* trichomes to cells with a cell height less than 40 μm. Given the frequent abnormal expansion of the stalk in *dis2*, this value is comparable to the threshold of approximately 25 μm that distinguishes the height of stage 4 and stage 5 wild-type cells (Figure 1 in Szymanski *et al.*, 1999). Because of cell to cell variation in the efficiency of actin filament labeling, the total integrated intensity of the cytoplasmic actin filament signal was used as an internal control. The phalloidin signal was dependent on actin filaments because cells treated with high concentrations of the actin filament-depolymerizing drug latrunculin B had background levels of fluorescence. The ratio of the integrated intensity of actin filaments in the core cytoplasm to that of the total cross-sectional area was calculated for *dis2-1* and wild-type branches. Although the mutant cells had a cell-swelling phenotype, we did not detect a difference between *dis2-1* and the wild type in stage 3/4 branches (Figure 7a). In stage

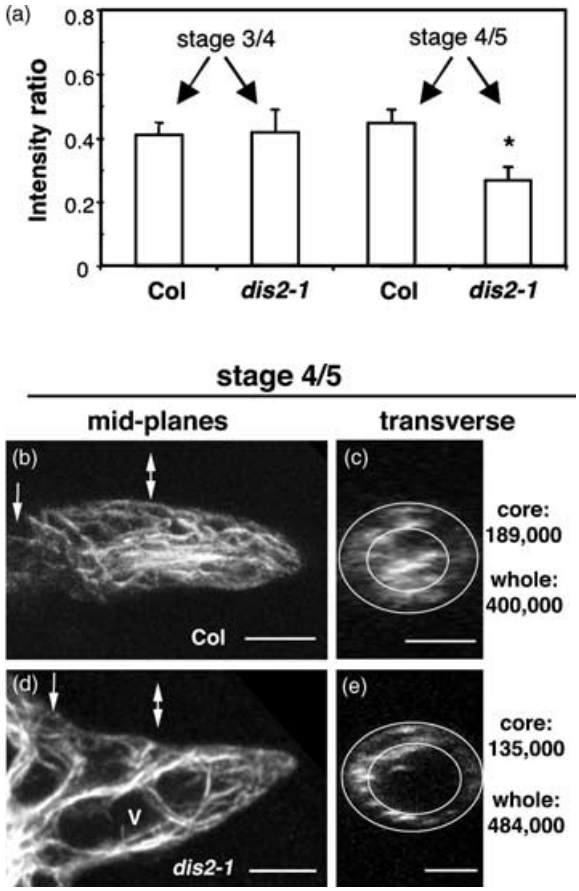

Figure 7. Quantification of the relative amounts of core cytoplasmic actin filaments in wild-type and *dis2-1* trichome branches.
(a) Ratios of core cytoplasmic to total cytoplasmic actin filament signal in developing stage 3/4 and stage 4/5 branches. Values are the mean ratios ± SD from 5 to 10 branches. Asterisk indicates a significant difference after two-tailed *P*-value *t*-test ($P < 0.0001$).
(b–d) Representative maximum projections of longitudinal views and transverse cross-sectional views of the core cytoplasm.
(b, c) Wild type; (d,e) *dis2-1*.
Transverse views were used for quantification. (b,d) Projections of longitudinal sections encompassing the core cytoplasm; (c,e) projections of transverse sections from the midpoint of the branch (0.5L). Ovals are example regions of interest that define whole and core cytoplasmic space; numbers are measured integrated intensity values. Bars = 5 μm. Arrows indicate the branch base. Double-headed arrows label the branch midpoint (0.5L). V, vacuole.

4/5 *dis2-1* branches, the relative amount of core actin filaments was significantly reduced compared to the wild type (Figure 7a). Representative images of the longitudinal and transverse views of the input data for the wild type (Figure 7b,c) and *dis2-1* (Figure 7d,e) are shown.

Stage 5 wild-type trichomes have highly elongated branches with a pointed tip morphology. Wild-type trichomes at this stage had extensive cortical and cytoplasmic actin cytoskeletons that were loosely aligned with the long axis of the stalks and branches (Figure 8a–c). Similarly staged *dis2-1* trichomes had a more randomly oriented cortical actin cytoskeleton, and the severity of the disorganization correlated with the extent of swelling for a particular cell (Figure 8d). We consistently observed dense populations of actin filaments and/or fine bundles in the cytoplasm of *dis1* (D. Szymanski and J. Lie unpublished results) and *dis2-1* trichomes (Figure 8e,f). The *dis2* vacuoles are highly convoluted compared to the wild type (D. Szymanski and J. Le, unpublished results). Therefore, the cytoplasmic networks of actin filaments in late-stage 'distorted group' trichomes may reflect an altered vacuole shape (Mathur *et al.*, 2003b) rather than the direct effect of the mutation. The abnormal random organization of cortical actin filaments and the intricate arrays of *trans*-vacuolar filaments persisted in the stalks of swollen stage 6 *dis2-1* trichomes relative to similarly staged wild-type cells (Figure 8g–l). High-magnification images of cytoplasmic bundles in *dis2* stage 5 (Figure 8f) and stage 6 (Figure 8l) trichomes failed to detect increased filament bundling compared to the wild type. These localization patterns differ from the highly bundled arrangement of filaments that has been observed in late-stage distorted trichomes using GFP-talin as a probe (Li *et al.*, 2003; Mathur *et al.*, 2003a,b).

Discussion

DIS2 encodes a protein with ARPC2 activity

Several 'distorted group' genes encode putative subunits of an *Arabidopsis* ARP2/3 complex and constitute a useful set of mutants to better understand the mechanisms of actin-dependent growth. Strong molecular genetic data presented here demonstrate the importance of an *ARPC2*-like gene during *Arabidopsis* epidermal development. We sequenced three independent alleles of *dis2* that affected the coding information of the *ATARPC2A* gene. Furthermore, we were able to restore a wild-type trichome phenotype to *dis2* plants by overexpressing the wild-type *DIS2* cDNA. Therefore, *ATARPC2A* can be included with *ATARP2*, *ATARP3*, and *ATARPC5* (Le *et al.*, 2003; Li *et al.*, 2003; Mathur *et al.*, 2003a,b) in the list of ARP2/3 subunit-like genes that control cell and tissue morphogenesis.

Despite the moderate level (approximately 30%) of sequence identity with the yeast ARPC2 subunit, DIS2 could rescue the growth defects of *arc35Δ* (*aprc2*) yeast cells (Figure 4). The functional similarity between DIS2 and known ARPC2 subunits also includes a conserved physical interaction that occurs between ARPC2 and ARPC4 (Gournier *et al.*, 2001; Zhao *et al.*, 2001). Based on the crystal structure of the ARP2/3 complex, the C-terminal domain of vertebrate ARPC2 forms an extended alpha-helix that makes multiple contacts with ARPC4 (Robinson *et al.*, 2001). Perhaps these interactions with ARPC4 more tightly

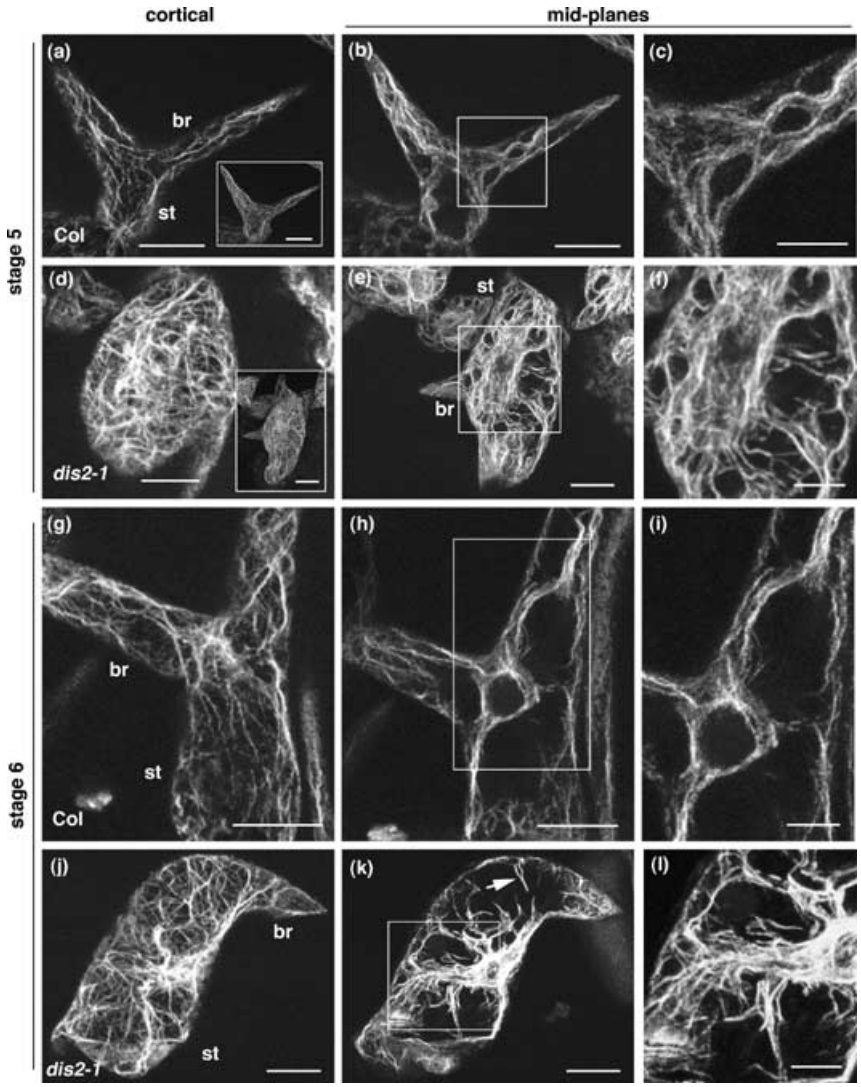

Figure 8. Actin localization in wild-type and *dis2-1* trichomes at late stages of cell expansion (stage 5) and in mature trichomes (stage 6).
(a–f) Maximum projections of stage 5 trichomes. (a–c) Wild type; (d–f) *dis2-1*.
(g–l) Maximum projections of stage 6 trichomes. (g–i) Wild type. (j–l) *dis2-1*.
Maximal projections of the cortical actin cytoskeleton; insets are projections of the standard deviation of the pixel values for all planes to give a clearer depiction of the whole-cell actin organization (a,d,g,j). Maximum projections of actin filaments in the planes that bisect the trichomes longitudinally (b,e,h,k).
(c, f, i, l) Detail of the highlighted regions of panels (b,e,h,k, respectively).
Bars: (a,b,d,e,g,h,j,k) 20 μm; (c,f,i,l) 10 μm. br, Branch; st, stalk. Arrow indicate the *trans*-vacuolar bundles.

constrain the C-terminal amino acid sequence of DIS2 and ATARPC2B (Figure 3). The *dis2-2* and *dis2-3* alleles introduce nonsense mutations that remove the conserved C-terminal domain, and provide additional evidence for its importance. Although the first 140 amino acids of human ARPC2 are dispensable for a two-hybrid interaction with ARPC4 (Zhao *et al.*, 2001), amino acids 166–191 of DIS2 appear to be important. The *dis2-1S* allele deletes amino acids 166–191, and in a two-hybrid assay, dis2-1S had a weakened interaction with ATARPC4 (Figure 4b). Although the dis2-1S fusion proteins accumulated in yeast, the reduced two-hybrid interaction could be because of improper protein folding. Alternatively, the failure of dis2-1S to interact normally with ARPC4 may explain its inability to function in yeast and plant cells.

In addition to DIS2, *Arabidopsis* encodes a second *ARPC2*-like gene that we named *ATARPCB* (Le *et al.*, 2003). ATARPC2B shares a similar level of amino acid identity with other ARPC2s, but includes an additional 60 amino acids at the C-terminus. The rice genome also encodes two *ARPC2*-like genes, one of which encodes a C-terminal extension that is similar to that of *ATARPC2B*. Phylogenetic analyses of the plant ARPC2-like protein sequences support an evolutionary model in which the *ARPC2A* and *ARPC2B* genes arose from a common ancestral gene that duplicated prior to the divergence of monocots and dicots. One possibility is that *ARPC2A* and *ARPC2B* paralogs evolved distinct functions. There is evidence in budding yeast for genetically separable ARPC2 (ARC35) functions. Temperature-sensitive mutations in ARC35 cause defects both in mitotic progression and in the organization of the actin cytoskeleton (Schaerer-Brodbeck and Riezman, 2000). The cell cycle- and actin-based phenotypes are rescued by overexpression of different mutant forms of calmodulin. Based on the presence of a strong candidate calmodulin-binding domain in the C-terminal extension of

ATARPC2B (D. Szymanski, unpublished results), it is possible that this protein is uniquely regulated by calmodulin. Future studies will determine if ATARPC2B is required for trichome morphogenesis.

Trichome and actin phenotypes of dis2

During stage 4, the aspect ratio of the branch increases and the tip morphology transitions from a hemi-spherical dome to a fine point. The microtubule and actin cytoskeletons are required during this transition, but cause distinct cell shape defects when they are disrupted with inhibitors (Szymanski, 2001). The stage 4-specific swelling of *dis2* trichomes is indistinguishable from actin-disrupted cells, and demonstrates the importance of the wild-type gene during branch elongation. Following branch initiation, *dis2* trichomes expanded in an unpredictable but polarized manner in the branches, stalk, or the interbranch zone (Figure 1). This suggests that the cortex and walls of stage 4 and 5 trichomes are uniformly capable of supporting cell expansion, and 'distorted group' genes are required to maintain a normal pattern of polarized growth and branch elongation. However, the precise relationship between ARP2/3 subunit function, the organization of actin, and the maintenance of polarized growth is not known.

If mutations in 'distorted group' genes reduce the actin filament-nucleating activity of a plant ARP2/3 complex, one expects to find altered actin structures at the onset of the mutant phenotype. At this stage of development, there is no published data available using GFP-talin, but in chemically fixed wild-type samples, bundles of actin filaments are clearly aligned with the long axis of the branch (Le *et al.*, 2003; Szymanski *et al.*, 1999). In *dis2* trichome branches, the relative amount of actin filaments in the core cytoplasm is unaltered, but many of the bundles are not aligned with the long axis (Figure 7). Rather than terminating cleanly within the core cytoplasm, many cytoplasmic *dis2* bundles were traced to cortical regions or meandered toward and within the stalk in an apparently random fashion. DIS2-dependent cytoplasmic bundles may form by a known ARP2/3-dependent mechanism. In an *in vitro* reconstitution assay (Vignjevic *et al.*, 2003), the balanced activity of ARP2/3-dependent nucleation and fascin-dependent bundling generates parallel, bundled actin filaments. In this assay system, ARP2/3 localizes to the pointed or minus end of the actin bundles (Vignjevic *et al.*, 2003). Although *Arabidopsis* does not encode a fascin homolog, plant actin cross-linking proteins such as villin (Klahre *et al.*, 2000) and/or fimbrin (Kovar *et al.*, 2000) may function in concert with an ARP2/3 complex to generate highly organized actin bundles in developing branches. Alternatively, the randomly oriented bundles in *dis2* and other 'distorted group' mutants may be an indirect effect of altered trafficking or organelle biogenesis. In the budding yeast, ARP2/3 subunit genes are required for endocytosis (Moreau *et al.*, 1997), mitochondrial motility (Boldogh *et al.*, 2001), and vacuole morphogenesis (Eitzen *et al.*, 2002). In this scenario, *DIS2*-dependent filament arrays in the core cytoplasm may promote organelle transport or fusion events that are required to generate a population of polarized bundles. Co-localization of ARP2/3 subunits with actin, candidate actin bundling proteins, and different endomembrane compartments will provide important functional clues.

The function of the core cytoplasmic bundles during branch elongation is not known. However, in developing branches, the core cytoplasm is dominated by an acropetal gradient of vacuolar fusion (D. Szymanski and J. Le, unpublished results). Perhaps core cytoplasmic bundles play a structural role and regulate trafficking to vacuole compartments or their positioning. In developing *dis1* and *dis2* trichomes, the vacuole frequently invades the branch, and may explain the reduced relative amounts of core actin filaments in stage 4/5 trichomes (Figure 7). Stable association of the actin cytoskeleton with subregions of the tonoplast would have the benefit of mechanically protecting cytoplasmic domains from the intrusion of an expanding central vacuole. Alternatively, DIS2-dependent actin filaments may push on the tonoplast during its biogenesis. In plant cells, some aspects of vacuole dynamics are actin dependent (Uemura *et al.*, 2002), and in yeast, both actin polymerization and ARP2/3 subunits are required for vacuole biogenesis (Eitzen *et al.*, 2002). Although distorted mutants have highly fused vacuoles (D. Szymanski, unpublished results), there may be multiple fusion pathways, only a subset of which display ARP2/3 subunit-dependence. Again, localization studies will help to distinguish between these different potential functions.

Essential functions for the Arabidopsis *ARP2/3 complex?*

Known ARP2/3 subunit mutants in *Arabidopsis* have only subtle effects on whole plant architecture and growth, and differ markedly from the severe developmental defects that occur when essential subunit function is compromised in *Drosophila* (Hudson and Cooley, 2002) and *C. elegans* (Sawa *et al.*, 2003). Although actin filament levels have not been measured directly, all localization data suggest that polymer levels in trichomes are relatively insensitive to ARP2/3 subunit function. The filaments in *dis2* trichomes may arise from residual *dis2* and/or ARP2/3 complex activity. Yeast *arc35Δ* (*arpc2*) cells contain de-stabilized but partially functional complexes (Winter *et al.*, 1999). The extent to which *ATARPC2B* can substitute for *DIS2* is another unknown factor: it may be that much of the actin detected in *dis2* reflects the functional redundancy of the paralogue. It seems more likely that ARP2/3 subunit-dependent nucleation is not the predominant pathway in plant

cells. Formins are a recently identified class of actin filament-binding proteins that promote polymerization (Kovar *et al.*, 2003; Pruyne *et al.*, 2002), and genetic tests in yeast place formin function upstream from ARP2/3 (Evangelista *et al.*, 2002). Perhaps the family of *Arabidopsis* formin-like genes (Cvrckova, 2000; Deeks *et al.*, 2002) generates the majority of actin filaments. Although it was mentioned that *dis1* (*apr3*) *wrm* (*arp2*) double mutants did not have an enhanced phenotype (Mathur *et al.*, 2003a), an array of double mutants and reagents to monitor the assembly status and activity of an ARP2/3 complex are needed to directly test for essential functions.

Regardless of whether or not ARP2/3 subunits are essential, they affect growth throughout plant development. *DIS2* and other ARP2/3-subunit genes were expressed in several major organs, *dis2* plants have reduced shoot growth, and the cell–cell adhesion is misregulated in several tissues. For example, *dis2* cotyledon and hypocotyl epidermal cells had cell–cell adhesion defects (Supplementary Material, Figure S1). The gaps between adjacent epidermal cells were similar to, but not as severe as those seen in *quasimodo1* (*qua1*) and *spike1* (*spk1*) plants. *QUA1* encodes a putative membrane-bound pectin biosynthetic enzyme (Bouton *et al.*, 2002) and *SPK1* (Qiu *et al.*, 2002), a putative activator of plant-specific Rho-GTPases, termed ROPs (Rho of plants). It will be interesting to find out which cell compartments and gene functions directly regulate the physical interactions among epidermal cells. In animal cells, ARP2/3 dendritic actin drives membrane protrusion. To our knowledge, there is no evidence to support a similar activity in plant cells. The growth of tip-growing root hairs (Baluska *et al.*, 2000) and pollen tubes (Gibbon *et al.*, 1999) is actin dependent, but is relatively insensitive to ARP2/3 subunit mutations. Perhaps in plant cells, turgor force provides the energy needed to push the plasma membrane forward during cell expansion, and ARP2/3-dependent actin filament nucleation is used elsewhere in the cell to distort membrane surfaces.

Conclusion

The ARP2/3 complex is a key regulatory module in the nucleation of actin filaments. In animal and yeast cells, diverse signaling pathways impinge upon the ARP2/3 complex to regulate plasma membrane protrusion, endocytosis, and organelle motility. The 'distorted group' is a useful set of mutants to test for multiple functions of plant ARP2/3 subunits in the context of multicellular development. This and a previous paper (Le *et al.*, 2003) focused on *DIS1* (*ARP3*)- and *DIS2*-dependent polarized actin bundles in the core cytoplasm. Considering the ARP2/3 dependence of endocytosis in budding yeast and the widespread homology between the *Arabidopsis* and yeast endocytic machinery (Holstein, 2002), it will be important to test for DIS2- and actin-dependent functions at the plasma membrane. Questions also linger concerning the nature of a plant ARP2/3 complex. The similar phenotypes of the 'distorted group' mutants, the activity of *DIS2* and *DIS1* (*ARP3*) in yeast, and a complete set of expressed *Arabidopsis* ARP2/3 subunit genes strongly suggest that some sort of ARP2/3 complex exists. However, it is not known if mutations in each of the ARP2/3 subunit-like genes can cause a distorted trichome phenotype, and it is not known if the subunits assemble into a seven-protein complex with nucleation activity. Proof of the existence of a seven-protein ARP2/3 complex awaits further genetic and biochemical experiments. Last, if the putative plant ARP2/3 complex is regulated like other known complexes, it will require signal transduction and *trans*-activating proteins to promote nucleation. However, clear homologs of evolutionarily conserved, signaling proteins like Wiskott-Aldrich syndrome protein (WASP) are not present in the *Arabidopsis* genome sequence. If there is a novel plant ARP2/3 activator(s), cloning of unknown 'distorted group' genes may reveal its identity.

Experimental procedures

Plant strains and growth conditions

dis2-1 (L*er*) was obtained from the Arabidopsis stock center and out-crossed to Col-0 five times prior to use. *dis2-2* and *dis2-3* were recovered from a methane sulfonic acid, ethyl ester (EMS)-mutagenized Col-0 population using standard protocols (this study). Allelism tests were performed using *dis2-1* as the common parent. For SEM and FW measurement, seedlings were grown on soil under continuous illumination (110 μmol) at 25°C. For localization experiments, plants were grown *in vitro* on 0.5× MS plates at 24°C under continuous illumination (120 μmol).

DIS2 *allele characterization and* dis2 *rescue*

To generate PCR products for the *DIS2* sequencing, we used two pairs of primers (DIS2_F1/DIS2_R4 and DIS2_F4/DIS2_R1). The *DIS2* coding region was sequenced using eight forward primers (DIS2-F1 to DIS2-F8) and eight reverse primers (DIS2-R1 to DIS2-R8). The *DIS2* templates and primer sequences are in Supplementary Material (Figure S3). The *dis2-1* (L*er*) genomic DNA sequence was compared with the sequence of the *ATARPC2* gene that was sequenced in the wild-type L*er* background. DNA sequencing was performed using the Bigdye mix (PE Biosystems, Foster City, CA, USA), and unincorporated nucleotides were removed with Centriflex TM gel filtration cartridge (Edge Biosystems, Gaithersburg, MD, USA). Sequencing reactions were analyzed at the Purdue Genomics Center. To generate the *DIS2* overexpression construct for rescue experiments, pEN-DIS2 was recombined into the binary Gateway 35S viral expression vector pGWB2 (a gift from Tsuyoshi Nakagawa, Research Institute of Molecular Genetics, Shimane University, Japan) to yield pGWB2-DIS2. pGWB2-DIS2 was used to transform *dis2-1* using *Agrobacterium*-mediated transformation. Phenotypic rescue was observed in T_1 seedlings, and the rescue activity segregated in T_2 populations.

RT-PCR

Total RNA for RT-PCR was isolated using the RNeasy plant mini kit from Qiagen (Chatsworth, CA, USA). All RNA extractions and RT-PCR analyses were repeated at least two times. Five micrograms of total RNA was treated with 5 units of RQ1 RNase-Free DNase (Promega, Madison, WI, USA). For the first-strand 25-μl cDNA synthesis reactions, total RNA was annealed with random hexanucleotides (20 ng μl^{-1}; New England Biolabs, Beverly, MA, USA), and then reverse transcribed with 200 units of M-MLV RT (Invitrogen, Carlsbad, CA, USA). Thereafter, 1/25 volume of the cDNA was used as a template for PCR. To analyze the effects of the *dis2* alleles, we used C2A-F primer (5′-CTGTGACAGAGAATGTCG-GTCGT-3′), and C2A-R primer (5′-AAAATACATGTCTCAGCTAAT-CACAAG-3′). To analyze the expression of some of the *Arabidopsis* ARP2/3 subunit genes in different tissues, we isolated organs from five DAG seedlings, 15 DAG seedlings, stems, inflorescences, and flowers from Col-0 plants. Gene names, primer sequences, and product sizes are listed in the Supplementary Material (Figure S4).

Sequence comparisons and phylogenetic analyses

ARPC2 amino acid sequences from *Arabidopsis* DIS2 (GenBank Accession: BT005308), ATARPC2B (GenBank Accession: NM_179877), *Oryza sativa* OSARPC2A (GenBank Accession: AP003709), OSARPC2B (GenBank Accession: CAE03390), *Bos taurus* BTARPC2 (GenBank Accession: 1K8K_D), *Drosophila melanogaster* DMARPC2 (GenBank Accession: NP_610033), *C. elegans* CEARPC2 (GenBank Accession: NP_741088), and *S. cerevisiae* SCARPC2 (GenBank Accession: NP_014433) were aligned using CLUSTALW. In CLUSTALW, the gap-opening and gap-extension penalties were set at 0.20 and 12, respectively, and the alignment was refined manually. A maximum parsimony tree was constructed using Phylogenetic Analysis Using Parsimony (PAUP), version 4.0, using Bootstrap as a re-sampling method. The number of bootstrapping pseudoreplicates was 1000 using the branch-and-bound search.

S. cerevisiae arc35Δ *rescue*

The *S. cerevisiae* Arc35 deletion obtained from Resgen (Invitrogen) was sporulated to generate the haploid *arc35Δ* strain. The 957-bp *DIS2* coding region and the *dis2-1S* cDNA that deleted amino acids 166–191 were amplified from cDNA using primers 5′-CACCATAATGATACTATTGCAGTCACATTC-3′ and 5′-CTACTTC-GAGTTGGTGTGATTGACCTCG-3′ and cloned into the pENTR/D/TOPO vector (Invitrogen) to generate pEN-DIS2 and pEN-dis2-1S. These clones were sequenced, and then recombined into the yeast galactose-inducible vector pYES-DEST52 (Invitrogen), yielding pDS52-DIS2 and pDS52-dis2-1S. These constructs were then transformed into *arc35Δ* using the lithium acetate method (Ausubel *et al.*, 1994).

Yeast two-hybrid assays

The 507-bp *ATARPC4* cDNA was amplified using primers 5′-CACCGCAAACTCATTACGGCTGTATC-3′ and 5′-TTACATGAACT-GTTTCAAGAAC-3′ and cloned into pENTR/D/TOPO vector (Invitrogen) to generate pEN-ARPC4. This clone was then sequenced and recombined into the yeast two-hybrid vector pDEST32 to generate pDS32-ARPC4 (bait). pEN-DIS2 and pEN-dis2-1S were cloned in-frame into the yeast two-hybrid vector pDEST22 to generate pDS22-DIS2 (prey) and pDS22-dis2-1S (prey), which were co-transformed with pDS32-ARPC4 into *S. cerevisiae* Y190 strain. The transformants were selected on Leu^- Trp^- medium. Two-hybrid interaction was determined by colony formation on Leu^- Trp^- His^- medium using *HIS3* reporter gene. For each set of constructs, liquid β-galactosidase assays were performed in triplicate from three independent colonies using standard protocols (Ausubel *et al.*, 1994).

F-actin localization and quantification

F-actin localization and quantification methods were similar to those described by Le *et al.* (2003). Tissues were fixed at room temperature in 2% formaldehyde in 100 mM piperazine-*N*,*N*′-bis-[2-ethane sulfonic acid] (PIPES)-KOH, pH 6.9, 5 mM EGTA, 4 mM $MgCl_2$ (PEM) for 30 min. After two washes with PEM, the tissues were incubated in PEM containing 1% glycerol and 0.2 μM Alexa Fluor® 488 phalloidin (Molecular Probes Inc., Eugene, OR, USA) overnight at 4°C. Images were collected using an MRC Bio-Rad 2100 confocal microscope with a Nikon 60× Plan Apo (numerical aperature (NA) 1.2) water immersion objective. Images were processed and analyzed using METAMORPH (Universal Imaging Corp., Downingtown, PA, USA) or IMAGEJ (available at web site of http://rsb.info.nih.gov/ij) software. The relative amount of core cytoplasmic actin filaments to total actin filaments in developing trichomes was measured at different developmental stages. Branches between 10 and 15 μm in length were defined as stage 3/4 and those between 16 μm and 50 μm in length were defined as stage 4/5. Trichomes greater than 40 μm in height were not used in the assay. Image stacks of branches with the long axis parallel to the *XY* plane were rotated to a direction parallel to the *X*- or *Y*-axis. Orthogonal views (*YZ* or *XZ*) were generated using METAMORPH software. The position of the middle orthogonal plane of each branch was defined at one-half of the total branch length (0.5L). For each branch, transverse sections 1.3 μm distal and proximal from the 0.5L plane were quantified. A 2.5-μm-wide band inside the plasma membrane of each transverse section was defined as 'cortical' cytoplasm. Cytoplasmic space not included within the outer 2.5-μm band was defined as 'core' cytoplasm (see Figure 7). Whole cytoplasmic space was the 'core' plus 'cortical'. Total integrated fluorescence intensity was measured within the core and whole cytoplasmic space, and the ratio of core to whole cytoplasmic signal was calculated for each transverse optical section. Between 15 and 30 planes were measured individually, and then averaged, for each branch. The ratios reported in Figure 7 were averaged from 5 to 10 branches.

Acknowledgements

Thanks to Cliff Weil for helpful comments on the manuscript and to Ray Zielinski for helping with the calmodulin-binding domain prediction. We are indebted to Gregore Koliantz for help in coordinating mutant screens and conducting complementation tests. Mohamed Saad constructed the full-length ATARPC4 clone that was used for yeast expression. Thanks to the Purdue Genomics Center and Phillip SanMiguel for DNA sequencing. The Arabidopsis stock center provided BAC clone T17H7. This work was supported by National science foundation grant 0110817-IBN, Department of Energy grant DE-FG02-02ER15357, and a Purdue Agricultural Research Program fellowship to D.B.S.

Supplementary Material

The following material is available from http://www.blackwellpublishing.com/products/journals/suppmat/TPJ/TPJ2065/TPJ2065sm.htm

Images of the hypocotyl defects in *dis2-1* etiolated seedlings and the phylogenetic tree of ARPC2s from several species are included as Supplementary Material. The sequence and position of primers used for allele sequencing, RT-PCR, and clone confirmation are listed in tabular format. The sizes of RT-PCR products corresponding to each primer pair are also listed.

Figure S1. Defects of epidermal cells at the mid-zone of 6-day-old dark-grown *dis2-1* hypocotyls.

(a) Epidermal cells at middle of the wild-type hypocotyls.

(b) Epidermal cells of *dis2-1* hypocotyls grown under the same conditions; Inset, detail of curling end of epidermal cell in the same panel. Scale bars = 100 μm.

Figure S2. Predicted phylogenetic relationships among ARPC2 proteins from different kingdoms.

The gene products and Accession numbers are: DIS2 (BT005308), ATARPC2B (NM_179877), *O. sativa* OSARPC2A (AP003709), OSARPC2B (CAE03390), *B. taurus* BTARPC2 (1K8K_D), *D. melanogaster* DMARPC2 (NP_610033), *C. elegans* CEARPC2 (NP_741088), and *S. cerevisiae* SCARPC2 (NP_014433).

Figure S3. *DIS2* mutant allele sequencing primers.

(a) Arrows indicate the forward and reverse primers that were used for *DIS2* sequencing.

(b) The names and sequences of the primers.

Figure S4. RT-PCR primers and product sizes for each of the ARP2/3 subunit-like genes.

References

Amann, K. and Pollard, T. (2001) Direct real-time observation of action filament branching mediated by Arp 2/3 complex using total internal reflection fluorescence microscopy. *Proc. Natl. Acad. Sci. USA*, **98**, 15009–15013.

Ausubel, F.M., Brent, R., Kingston, R.E., Moore, D.D., Seidman, J.G., Smith, J.A. and Struhl, K. (1994) *Current Protocols in Molecular Biology*. New York, NY: John Wiley & Sons.

Baluska, F., Salaj, J., Mathur, J., Braun, M., Jasper, F., Samaj, J., Chua, N.H., Barlow, P.W. and Volkmann, D. (2000) Root hair formation: F-actin-dependent tip growth is initiated by local assembly of profilin-supported F-actin meshworks accumulated within expansin-enriched bulges. *Dev. Biol.* **227**, 618–632.

Blancaflor, E.B. (2000) Cortical actin filaments potentially interact with cortical microtubules in regulating polarity of cell expansion in primary roots of maize (*Zea mays* L.). *J. Plant Growth Regul.* **19**, 406–414.

Blanchoin, L., Amann, K.J., Higgs, H.N., Marchand, J.B., Kaiser, D.A. and Pollard, T.D. (2000) Direct observation of dendritic actin filament networks nucleated by Arp2/3 complex and WASP/Scar proteins. *Nature*, **404**, 1007–1011.

Boevink, P., Oparka, K., Santa Cruz, S., Martin, B., Betteridge, A. and Hawes, C. (1998) Stacks on tracks: the plant Golgi apparatus traffics on an actin/ER network. *Plant J.* **15**, 441–447.

Boldogh, I.R., Yang, H.C., Nowakowski, W.D., Karmon, S.L., Hays, L.G., Yates, J.R. and Pon, L.A. (2001) Arp 2/3 complex and actin dynamics are required for actin-based mitochondrial motility in yeast. *Proc. Natl. Acad. Sci. USA*, **98**, 3162–3167.

Bouton, S., Leboeuf, E., Mouille, G., Leydecker, M.T., Talbotec, J., Granier, F., Lahaye, M., Hofte, H. and Truong, H.-N. (2002) *QUASIMODO1* encodes a putative membrane-bound glycosyltransferase required for normal pectin synthesis and cell adhesion in *Arabidopsis*. *Plant Cell*, **14**, 2577–2590.

Burk, D.H., Liu, B., Zhong, R., Morrison, W.H. and Ye, Z.H. (2001) A Katanin-like protein regulates normal cell wall biosynthesis and cell elongation. *Plant Cell*, **13**, 807–827.

Cvrckova, F. (2000) Are plant formins integral membrane proteins? *Genome Biol.*, **1**, research001.001–research001.007.

Deeks, M.J., Hussey, P.J. and Davies, B. (2002) Formins: intermediates in signal-transduction cascades that affect cytoskeletal reorganization. *Trends Plant Sci.* **7**, 492–498.

Eitzen, G., Wang, L., Thorngren, N. and Wickner, W. (2002) Remodeling of organelle-bound actin is required for yeast vacuole fusion. *J. Cell Biol.* **158**, 669–679.

Evangelista, M., Pruyne, D., Amberg, D.C., Boone, C. and Bretscher, A. (2002) Formins direct Arp2/3-independent actin filament assembly to polarize cell growth in yeast. *Nat. Cell Biol.* **4**, 260–269.

Feenstra, W.J. (1978) Contiguity of linkage groups I and IV as revealed by linkage relationship of two newly isolated markers *dis-1* and *dis-2*. *Arab. Inf. Serv.* **15**, 35–38.

Foissner, I., Lichtscheidl, I.K. and Wasteneys, G.O. (1996) Actin-based vesicle dynamics and exocytosis during wound wall formation in Characean internodal cells. *Cell Motil. Cytoskeleton*, **35**, 35–48.

Folkers, U., Kirik, V., Schöbinger, U. *et al.* (2002) The cell morphogenesis gene *ANGUSTIFOLIA* encodes a CtBP/BARS-like protein and is involved in the control of the microtubule cytoskeleton. *EMBO J.* **21**, 1280–1288.

Gibbon, B.C., Kovar, D.R. and Staiger, C.J. (1999) Latrunculin B has different effects on pollen germination and tube growth. *Plant Cell*, **11**, 2349–2363.

Gournier, J., Goley, E.D., Niederstrasser, H., Trinh, T. and Welch, M.D. (2001) Reconstitution of human Arp 2/3 complex reveals critical roles of individual subunits in complex structure and activity. *Mol. Cell*, **8**, 1041–1052.

Holstein, S.E. (2002) Clathrin and plant endocytosis. *Traffic*, **3**, 614–620.

Hudson, A.M. and Cooley, L. (2002) A subset of dynamic actin rearrangements in *Drosophila* requires the Arp2/3 complex. *J. Cell Biol.* **156**, 677–687.

Kirik, V., Grini, P.E., Mathur, J., Klinkhammer, I., Adler, K., Bechtold, N., Herzog, M., Bonneville, J.-M. and Hulskamp, M. (2002) The *Arabidopsis* TUBULIN-FOLDING COFACTOR A gene is involved in the control of the alpha/beta-tubulin monomer balance. *Plant Cell*, **14**, 2265–2276.

Klahre, U., Friederich, E., Kost, B., Louvard, D. and Chua, N.H. (2000) Villin-like actin-binding proteins are expressed ubiquitously in *Arabidopsis*. *Plant Physiol.* **122**, 35–48.

Kovar, D.R., Staiger, C.J., Weaver, E.A. and McCurdy, D.W. (2000) AtFim1 is an actin filament crosslinking protein from *Arabidopsis thaliana*. *Plant J.* **24**, 625–636.

Kovar, D.R., Kuhn, J.R., Tichy, A.L. and Pollard, T.D. (2003) The fission yeast cytokinesis formin Cdc12p is a barbed end actin filament capping protein gated by profilin. *J. Cell Biol.* **161**, 875–887.

Le, J., El-Assal, S.E., Basu, D., Saad, M.E. and Szymanksi, D.B. (2003) Requirements for *Arabidopsis ATARP2* and *ATARP3* during epidermal development. *Curr. Biol.* **13**, 1341–1347.

Lees-Miller, J.P., Henry, G. and Helfman, D.M. (1992) Identification of *act2*, an essential gene in the fission yeast *Schizosaccharomyces pombe* that encodes a protein related to actin. *Proc. Natl. Acad. Sci. USA*, **89**, 80–83.

Li, S., Blanchoin, L., Yang, Z. and Lord, E.M. (2003) The putative *Arabidopsis* Arp2/3 complex controls leaf cell morphogenesis. *Plant Physiol.* **132**, 2034–2044.

Machesky, L.M., Atkinson, S.J., Ampe, C., Vandekerckhove, J. and Pollard, T.D. (1994) Purification of a cortical complex containing two unconventional actins from *Acanthamoeba* by affinity chromatography on profilin-agarose. *J. Cell Biol.* **127**, 107–115.

Mathur, J., Spielhofer, P., Kost, B. and Chua, N. (1999) The actin cytoskeleton is required to elaborate and maintain spatial patterning during trichome cell morphogenesis in *Arabidopsis thaliana*. *Development*, **126**, 5559–5568.

Mathur, J., Mathur, N., Kernebeck, B. and Hulskamp, M. (2003a) Mutation in actin-related proteins 2 and 3 affect cell shape development in *Arabidopsis*. *Plant Cell*, **15**, 1632–1645.

Mathur, J., Mathur, N., Kirik, V., Kernebeck, B., Srinivas, B.P. and Hulskamp, M. (2003b) *Arabidopsis CROOKED* encodes for the smallest subunit of the ARP2/3 complex and controls cell shape by region specific fine F-actin formation. *Development*, **130**, 3137–3146.

Miller, D.D., de Ruijter, N.C.A., Bisseling, T. and Emons, A.M.C. (1999) The role of actin in root hair morphogenesis: studies with lipochito-oligosaccharide as a growth stimulator and cytochalasin as an actin perturbing drug. *Plant J.* **17**, 141–154.

Moreau, V., Galan, J., Devilliers, G., Haguenauer-Tsapis, R. and Winsor, B. (1997) The yeast actin-related protein Arp2p is required for the internalization step of endocytosis. *Mol. Biol. Cell*, **8**, 1361–1375.

Nebenfuhr, A., Gallagher, L.A., Dunahay, T.G., Frohlick, J.A., Mazurkiewicz, A.M., Meehl, J.B. and Staehelin, L.A. (1999) Stop-and-go movements of plant Golgi stacks are mediated by the acto-myosin system. *Plant Physiol.* **121**, 1127–1142.

Oppenheimer, D.G., Pollock, M.A., Vacik, J., Szymanski, D.B., Ericson, B., Feldmann, K. and Marks, M.D. (1997) Essential role of a kinesin-like protein in *Arabidopsis* trichome morphogenesis. *Proc. Natl. Acad. Sci. USA*, **94**, 6261–6266.

Pruyne, D., Evangelista, M., Yang, C., Bi, E., Zigmond, S.H., Bretscher, A. and Boone, C. (2002) Role of formins in actin assembly: nucleation and barbed-end association. *Science*, **297**, 612–615.

Qiu, J.L., Jilk, R., Marks, M.D. and Szymanski, D.B. (2002) The *Arabidopsis SPIKE1* gene is required for normal cell shape control and tissue development. *Plant Cell*, **14**, 101–118.

Robinson, R.C., Turbedsky, K., Kaiser, D.A., Marchand, J.-B., Higgs, H.N., Choe, S. and Pollard, T.D. (2001) Crystal structure of Arp 2/3 complex. *Science*, **294**, 1679–1684.

Sawa, M., Suetsugu, S., Sugimoto, A., Miki, H., Yamamoto, K. and Takenawa, T. (2003) Essential role of the *C. elegans* Arp2/3 complex in cell migration during ventral enclosure. *J. Cell Sci.* **116**, 1505–1518.

Schaerer-Brodbeck, C. and Riezman, H. (2000) *Saccharomyces cerevisiae* Arc35p works through two genetically separable calmodulin functions to regulate the actin and tubulin cytoskeletons. *J. Cell Sci.* **113**, 521–532.

Schafer, D.A. (2002) Coupling actin dynamics and membrane dynamics during endocytosis. *Curr. Opin. Cell Biol.* **14**, 76–81.

Schwab, B., Mathur, J., Saedler, R., Schwarz, H., Frey, B., Scheidegger, C. and Hulskamp, M. (2003) Regulation of cell expansion by the *DISTORTED* genes in *Arabidopsis thaliana*: actin controls the spatial organization of microtubules. *Mol. Genet. Genomics*, **269**, 350–360.

Seki, M., Narusaka, M., Kamiya, A. *et al.* (2002) Functional annotation of a full-length *Arabidopsis* cDNA collection. *Science*, **296**, 141–145.

Staiger, C.J. (2000) Signaling to the actin cytoskeleton in plants. *Annu. Rev. Plant Physiol. Plant Mol. Biol.* **51**, 257–288.

Szymanski, D.B. (2001) *Arabidopsis* trichome morphogenesis: a genetic approach to studying cytoskeletal function. *J. Plant Growth Regul.* **20**, 131–140.

Szymanski, D.B., Jilk, R.A., Pollock, S.M. and Marks, M.D. (1998) Control of *GL2* expression in *Arabidopsis* leaves and trichomes. *Development*, **125**, 1161–1171.

Szymanski, D.B., Marks, M.D. and Wick, S.M. (1999) Organized F-actin is essential for normal trichome morphogenesis in *Arabidopsis*. *Plant Cell*, **11**, 2331–2347.

Uemura, T., Yoshimura, S.H., Takeyasu, K. and Sato, M.H. (2002) Vacuolar membrane dynamics revealed by GFP-AtVam3 fusion protein. *Genes Cells*, **7**, 743–753.

Vignjevic, D., Yarar, D., Welch, M.D., Peloquin, J., Svitkina, T. and Borisy, G.G. (2003) Formation of filopodia-like bundles *in vitro* from a dendritic network. *J. Cell Biol.* **160**, 951–962.

Wasteneys, G.O. and Galway, M.E. (2003) Remodeling the cytoskeleton for growth and form: an overview with some new views. *Annu. Rev. Plant Biol.* **54**, 691–722.

Welch, M. and Mullins, D. (2002) Cellular control of actin nucleation. *Annu. Rev. Cell Dev. Biol.* **18**, 247–288.

Winter, D.C., Choe, E.Y. and Li, R. (1999) Genetic dissection of the budding yeast Arp 2/3 complex: a comparison of the *in vivo* and structural roles of individual subunits. *Proc. Natl. Acad. Sci. USA*, **96**, 7288–7293.

Zhao, X., Yang, Z., Qian, M. and Zhu, X. (2001) Interactions among subunits of human Arp2/3 complex: p20-Arc as the hub. *Biochem. Biophys. Res. Commun.* **280**, 513–517.